ISSN 2723-6471

Modeling Thermomechanical Effects in Rods with Variable Cross-Section and Local Heat Sources

Zhuldyz Tashenova[1], Shirin Amanzholova[2,*], Zhanat Abdugulova[3], Elmira Nurlybaeva[4]

[1,3]*Department of Information Technologies, L. N. Gumilyov Eurasian National University, Astana, Kazakhstan*

[2]*Department of Social and Humanitarian Disciplines, The Kurmangazy Kazakh National Conservatory, Almaty, Kazakhstan*

[4]*Department of Computer technologies, T.K. Zhurgenov Kazakh National Academy of Arts, Almaty, Kazakhstan*

(Received: February 1, 2026; Revised: April 2, 2026; Accepted:May 30, 2026; Available online: June 28, 2026)

Abstract

This study is a numerical study of the transient thermomechanical behavior of rods with variable cross-section exposed to partial thermal insulation, localized heat flows, and convective heat exchange. The main goal is to increase the accuracy and reliability of modeling related thermomechanical reactions in heterogeneous structural elements widely used in engineering applications. The main idea is based on the development of a mathematically consistent model based on the principle of conservation of energy, which allows simultaneous assessment of temperature fields and stress-strain state under inhomogeneous boundary conditions. The contribution of this work is to develop a computational algorithm capable of detecting spatial and temporal temperature changes and deformations with increased stability and efficiency. Numerical calculations show that the temperature along the rod varies non-linearly, reaching a maximum increase of about 18-25% near the zones of concentrated heat flow, while the thermal elongation differs by up to 12% compared with homogeneous models. The calculated stress values indicate an increase in peak thermal stresses by 20-30% in areas with a reduced cross-sectional area, which confirms the strong influence of geometric variability. Convergence analysis shows that reducing the sampling step by 50% increases the accuracy of the solution by about 8-10% while maintaining computational costs within acceptable limits (an increase of <15%). The results confirm that the proposed method provides stable solutions with an error of less than 5% compared to reference analytical solutions. The novelty of the research lies in the integration of variable geometry, mixed boundary conditions, and transient effects into a single numerical model that provides more realistic predictions than traditional simplified models. The results obtained can be effectively applied in the design and optimization of the main components operating under coupled thermomechanical loads.

Keywords: Heat Flow, Heat Transfer, Thermal Expansion Coefficient, Thermal Conductivity, Modulus of Elasticity

1. Introduction

Structural components of modern power-generating and high-temperature engineering systems—such as gas turbines, nuclear and thermal power plants, rocket and hydrogen engines, and advanced processing equipment—operate under complex coupled thermal and mechanical loads. The reliability and durability of these systems strongly depend on the accurate prediction of thermomechanical behavior in their load-bearing elements, many of which can be idealized as rods or rod-like structures. Classical approaches to thermoelastic analysis are largely based on continuum mechanics and heat transfer theory, where temperature fields are determined from energy conservation principles and subsequently used to evaluate stress–strain states [1], [2], [3], [4].

In recent decades, significant progress has been made in numerical modeling of thermomechanical processes using finite element methods and related computational techniques [5], [6], [7]. These approaches enable the analysis of transient temperature distributions and induced stresses under various boundary conditions, including convective heat exchange, internal heat generation, and localized thermal loading [8], [9], [10]. However, the majority of existing studies focus on rods with constant cross-sectional areas and relatively simplified boundary conditions, which limits their applicability to real engineering systems characterized by geometric non-uniformity and complex thermal interactions [11], [12], [13].

Despite these advances, there remains a lack of comprehensive models that simultaneously account for variable cross-sectional geometry, partial thermal insulation, and mixed boundary conditions involving both prescribed heat fluxes

*Corresponding author: Shirin Amanzholova (sh.amanzholova@gmail.com)
DOI: https://doi.org/10.47738/jads.v7i3.1340

ISSN 2723-6471

and convective heat transfer. In practical applications, such conditions are common and can significantly affect temperature gradients and stress distributions, leading to localized thermal stresses and potential structural failure. Therefore, there is a clear need for improved modeling approaches that can capture these combined effects with sufficient accuracy and computational efficiency [14], [15], [16].

The present study addresses this gap by developing a mathematical and computational framework for analyzing transient thermomechanical processes in rods of finite length with variable cross-sections under non-uniform thermal boundary conditions. The proposed approach is based on the principle of energy conservation and enables the determination of temperature distributions, thermal elongation, axial forces, and associated stress–strain fields. Unlike conventional models, the framework incorporates spatial variability of geometric properties together with partial insulation and localized heat fluxes within a unified formulation.

The novelty of this work lies in the integration of variable geometry and mixed thermal boundary conditions into a consistent numerical scheme that allows efficient evaluation of coupled thermomechanical responses. This contributes to enhancing the predictive capability of existing models and provides a more realistic representation of operating conditions in engineering structures. The results of this study are expected to support the design and optimization of rod-type components subjected to complex thermal and mechanical loading in advanced engineering applications.

2. Literature Review

Previous research, such as that in [1] and [2], has addressed the theory of elasticity and numerical methods in applied mechanics. The fundamental equations of thermophysics, as outlined in [3], encompass the conservation of mass, momentum, and energy. Studies in [4], [5], and [6] have examined contact heat transfer and the thermal stress–strain state under various conditions using the finite element method [7]. Additionally, works like [8] and [9] have investigated the stress–strain state in rigid plastic pipes and nonlinear finite element modeling, while [10] and [11] have discussed adiabatic shear bands and nonlinear continuum mechanics.

Research in [12] focused on the temperature distribution in nuclear fuel rods, underscoring the importance of fuel integrity. Meanwhile, [13], [14], and [15] derived computational relationships for thermal forces in rods with rectangular cross-sections. Other studies, such as [16], investigated the thermal behavior of bars during hot rolling. The finite element method was also applied in [17] and [18] to model temperature fields in Terfenol-D rods, while [19] explored unstable temperature distributions in cylindrical rods exposed to laser heating.

Significant contributions to the analysis of thermo-mechanical behavior of rod-like structures have been made in recent years, particularly in the development of analytical and numerical solution methods. In [20], Z. Tashenova and co-authors proposed a method and computational algorithm for solving stationary problems of rods under thermo-stressed conditions. This work established an effective framework for evaluating temperature-induced stresses while accounting for boundary conditions and material properties.

Further developments were presented in [21] and [22], where Z. H. M. Tashenova and collaborators introduced solution methods and computational algorithms for mixed thermo-mechanical problems. These studies emphasized the coupling between thermal and mechanical fields and demonstrated the applicability of numerical techniques for solving complex boundary-value problems. The proposed approaches improved the accuracy and stability of solutions, particularly in cases involving non-uniform temperature distributions.

In [23], a numerical investigation of the established thermo-mechanical state of rods was conducted, providing insights into the distribution of stresses and deformations under thermal loading. This study highlighted the importance of precise numerical modeling in predicting the behavior of structural elements subjected to combined thermal and mechanical effects. Complementary research in [24] extended the analysis to elastoplastic pipes, where temperature and compressibility effects were considered, demonstrating the broader applicability of thermo-mechanical models to more complex materials and geometries.

The theoretical basis for these studies is grounded in the principles of thermoelasticity, comprehensively described in Thermal Integrity in Mechanics and Engineering by B. F. Shorr. This work provides fundamental relations governing the interaction between thermal and mechanical fields. In parallel, the numerical implementation of such problems is largely based on the finite element method, as detailed in The Finite Element Method by O. C. Zienkiewicz and R. L. Taylor, which remains one of the most widely used tools for solving engineering problems involving complex geometries and boundary conditions.

 ISSN 2723-6471

Overall, the reviewed works [20], [21], [22], [23], [24], [25] , [26] demonstrate substantial progress in the modeling and analysis of thermo-mechanical systems. However, despite the effectiveness of existing methods, there remains a need for improved approximation techniques that can better capture localized thermal effects and enhance computational efficiency. This motivates the development of advanced approaches, such as the use of higher-order interpolation functions, for solving practical problems involving rods with variable cross-sections and complex thermal loading conditions.

3. Materials and Methods

Let us consider a rod of limited length clamped at two ends, the cross section of which varies along its length and is a circle. In this case, the radius of the section depends linearly on the coordinates. The radius of the left end is denoted by r_0, right end through r_L, and the length of the rod through L. Then the radius depends on the coordinate as follows [20].

$$r = \frac{r_L - r_0}{L} \cdot x + r_0 \tag{1}$$

Temperature is set at the left pinched end T(x=0)=T_1, on the right T(x=L)=T_(2n+1). Lateral surfaces of sections(0≤x≤x_1),(x_2≤x≤x_3) and(x_4≤x≤x_L). The rods are thermally insulated. Through the area of the lateral surface of the plot (x_1≤x≤x_2) heat exchange occurs with the environment. In this case, the heat transfer coefficient h, and the ambient temperature T_"co" . To the area of the lateral surface of the plot (x_3≤x≤x_4) a heat flux of constant intensity q is supplied. It is required to numerically study the influence of the value $T_0 \in [(-150\ C) \div (+150\ C)]$. The calculation scheme is shown in figure 1.

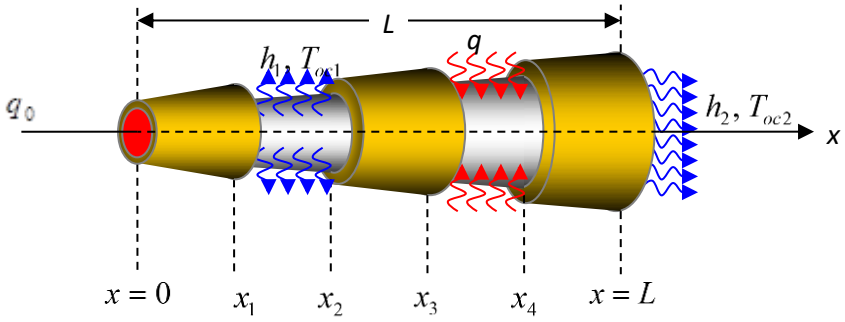

Figure 1. Calculation scheme of the problem

In this problem, based on the energy principle, it is necessary to develop a mathematical model of the temperature distribution field along the length of the rod, as well as its elongation due to thermal expansion. Based on the model, a corresponding computational algorithm, method and software package are developed that allow numerically investigating the thermomechanical state of partially heat-insulated rods of variable cross-section with the simultaneous presence of local heat flows and heat exchanges.

On the temperature distribution field $(T = T(x))$, elastic displacement $(u = u(x))$, as well as components of deformation $(\varepsilon_x = \varepsilon_x(x);\ \varepsilon_T = \varepsilon_T(x);\ \varepsilon = \varepsilon(x))$ and voltage $(\sigma_x = \sigma_x(x);\ \sigma_T = \sigma_T(x);\ \sigma = \sigma(x))$. In order to develop a mathematical model of the temperature distribution field along the length of the considered partially thermally insulated rod of limited length, it is discretized using quadratic elements with three nodes. The total number of elements will be n. Then the total number of nodes will be $(2n + 1)$. In this case, discretization is carried out in such a way that the boundaries of the elements coincide with the boundaries of the thermally insulated part of the rod. Next, for each element, a functional expression is written that characterizes its total thermal energy. In particular, for elements belonging to the thermally insulated part of the rod we have

$$I_i = \int_{V_i} \frac{K_{xx}}{2} \left(\frac{\partial T}{\partial x}\right)^2 \mathrm{dV}, (i = 1, 2, \ldots) \tag{2}$$

Where V_i- volume of the i-th element.

For elements located on the section of the rod through the areas of the lateral surface of which heat exchange occurs, the expression for the corresponding functional has the following form[22]

$$I_j = \int_{V_j} \frac{K_{xx}}{2}\left(\frac{\partial T}{\partial x}\right)^2 \mathrm{dV} + \int_{S_{jПБП}} \frac{h}{2}(T - T_{co})^2 \mathrm{dS}, (j = 1, 2, ...) \quad (3)$$

Where V_j- volume of the j-th element, $S_{jПБП}$- area of the lateral surface of the j-th element.

For elements located on a section of the rod, on the area of the lateral surface of which a heat flux of constant intensity q is supplied, the functional expression that characterizes their total thermal energy will be

$$I_k = \int_{V_k} \frac{K_{xx}}{2}\left(\frac{\partial T}{\partial x}\right)^2 \mathrm{dV} + \int_{S_{kПБП}} \mathrm{qT}(x)\mathrm{dS}, (k = 1, 2, ...) \quad (4)$$

General expression for the functional of total thermal energy for the considered partially thermally insulated rod of variable cross-section, taking into account the presence of local temperatures, heat flow and heat transfer

$$I = \sum_{t=1}^{n} I_t \quad (5)$$

By minimizing this functional based on the nodal temperature values, a mathematical model of the temperature distribution field along the length of the rod under study is constructed in the form of a resolving system of linear algebraic equations

$$\frac{\partial I}{\partial T_t} = 0, (t = 2, 3, ..., 2n) \quad (6)$$

Because T_1 and T_{2n+1} are considered given, then the number of equations in system (6) will be equal to$(2n + 1)$.

Solving the system for different values $T_1$and fixed values T_{2n+1}, h,T_{co}, as well as q, the influence of T_1 on the nature of the temperature distribution field along the length of the rod in question.[23]

After constructing the temperature distribution field along the length of the rod, a mathematical model of the distribution field of elastic displacement, as well as the components of deformation and stress, is constructed. To do this, the rod under study is discretized $\left(N = \frac{n}{2}\right)$ quadratic elements with three nodes. After which, for each element, an expression for the functional of the potential energy of elastic deformation is written, which has the form

$$\Pi_i = \int_{V_i} \frac{\sigma_x \varepsilon_x}{2} \mathrm{dV} - \int_{V_i} \alpha \mathrm{ET}(x)\mathrm{dV}, (i = 1, 2, ..., N) \quad (7)$$

V_i- volume of the i-th element,$u = u(x)$- elastic displacement distribution field, $\varepsilon_x = \frac{\partial u}{\partial x}$- distribution field of the elastic component of deformation, $\sigma_x = E\varepsilon_x = E \cdot \frac{\partial u}{\partial x}$- distribution field of the elastic component of stress, E - elastic modulus of the rod material, α- coefficient of thermal expansion of the rod material, $T = T(x)$- temperature distribution field determined from the solution of system (6).

For the considered rod as a whole, the expression for the potential energy of elastic deformation is as follows

$$\Pi = \sum_{i=1}^{N} \Pi_i \quad (8)$$

By minimizing the latter according to the nodal values of the elastic displacement, a mathematical model is constructed for the distribution of elastic displacement along the length of the rod under study in the form of the following system of linear algebraic equations[26]

$$\frac{\partial \Pi}{\partial u_i} = 0, (i = 1, 2, ..., (2N + 1)) \quad (9)$$

Solving this system, the elastic displacement distribution field is determined $u = u(x)$ along the length of the rod in question. Based on them, the corresponding fields for the distribution of the components of deformation and stress are constructed as follows:

$$\varepsilon_x = \frac{\partial u}{\partial x};\ \varepsilon_T = -\alpha T(x);\ \varepsilon = \varepsilon_x + \varepsilon_T \quad (10)$$

$$\sigma_x = E\varepsilon_x;\ \sigma_T = E\varepsilon_T;\ \sigma = (\sigma_x + \sigma_T) \quad (11)$$

In this problem, based on the energy principle, it is necessary to develop a mathematical model of the temperature distribution field along the length of the rod, as well as its elongation due to thermal expansion. Based on the model, a

corresponding computational algorithm, method and software package are developed that allow numerically investigating the thermomechanical state of partially heat-insulated rods of variable cross-section with the simultaneous presence of local heat flows and heat exchanges. To do this, for the problem under consideration, taking into account the heterogeneous boundary conditions, we first write down the expression for the total thermal energy.

$$I = \int_{S_0} q_0 T dS + \int_{V_1} \frac{K_{xx}}{2}\left(\frac{\partial T}{\partial x}\right)^2 dV + \int_{S_{ПБП2}} \frac{h_1}{2}(T - T_{co1})^2 dS + \int_{V_2} \frac{K_{xx}}{2}\left(\frac{\partial T}{\partial x}\right)^2 dV + \\ + \int_{V_3} \frac{K_{xx}}{2}\left(\frac{\partial T}{\partial x}\right)^2 dV + \int_{S_{ПБП4}} q_1 T dS + \int_{V_4} \frac{K_{xx}}{2}\left(\frac{\partial T}{\partial x}\right)^2 dV + \int_{V_5} \frac{K_{xx}}{2}\left(\frac{\partial T}{\partial x}\right)^2 dV + \\ + \int_{S_{ПБПL}} \frac{h_2}{2}(T - T_{co2})^2 dS \quad (12)$$

S_0- the cross-sectional area of the left end (x=0) of the rod to which the heat flow of intensity is suppliedq_0;V_1- volume of 1 section ($0 \le x \le x_1$) rod;$S_{ПБП2}$- the area of the lateral surface of the 2nd section ($x_1 \le x \le x_2$) the rod through which heat exchange occurs;V_2- volume of the 2nd section ($x_1 \le x \le x_2$) rod;V_3- volume of the 3rd section ($x_2 \le x \le x_3$) rod;$S_{ПБП4}$- the area of the lateral surface of the 4th section ($x_3 \le x \le x_4$) of the rod to which the heat flow of intensity is suppliedq_1;V_4- the volume of this section of the rod;V_5- volume of the 5th section ($x_4 \le x \le L$) rod;S_L- the cross-sectional area of the right end (x=L) of the rod, through which heat exchange with the environment surrounding this area occurs.

4. Results and Discussion

Taking into account the specifics of the problem within each section of the temperature distribution field, we approximate the full second-order polynomial $T(x) = \phi_i(x)T_i + \phi_j(x)T_j + \phi_k(x)T_k$. In this case, we represent each section as one quadratic element with three nodes. Then the total number of nodes in the rod will be eleven. We write the integrated form (12) with r_1,r_3,r_5,r_7,r_9- the radii of the rod, respectively, in sections whose coordinates$x = 0$,$x = x_1$,$x = x_2$,$x = x_3$ and $x = x_4$;ℓ_1,ℓ_2,ℓ_3,ℓ_4,ℓ_5- lengths of the corresponding sections;S_1,S_2,S_3,S_4,S_5; F_0- cross-sectional area of the left end (x=0) of the rod;F_ℓ- area of the right end (x=L).

Now, by minimizing I by the nodal temperature values, we obtain a resolving system of equations, the solution of which determines the field distribution of temperature along the length of the rod under consideration. To solve system (12), we will take the following as initial data:

$r_1 = 1(см), r_2 = 2(см), L = 20(см), x_1 = 4(см), x_2 = 8(см), x_3 = 12(см), x_4 = 16(см), \ell_1 = \ell_2 = \ell_3 = \ell_4 = \ell_5 = 4(см), q_0 = q_1 = -1000(Bm/см^2), h_1 = h_2 = 10(Bm/(см^2 \cdot {}^\circ C)), T_{co1} = T_{co2} = 40({}^\circ C), K_{xx} = 100(Bm/(см \cdot {}^\circ C)), \alpha = 125 \cdot 10^{-7}(1/{}^\circ C)$.

With these data, solving system (12) we find the nodal temperature values(table 1). Table 1 contains the calculated nodal temperature values for the rod, obtained by dividing the model into five finite elements and solving the system of equations (12) for the given initial parameters.

Table 1. Temperature value (number of quadratic elements in the rod NQE =5)

Node. dots	Temp. in knots points $T({}^\circ C)$	Node. dots	Temp. in knots points $T({}^\circ C)$	Node. dots	Temp. in knots points $T({}^\circ C)$	Node. dots	Temp. in knots points $T({}^\circ C)$
1	134,787	4	108,283	7	281,486	10	245,318
2	118,304	5	159,428	8	305,514	11	208,101
3	101,821	6	220,457	9	282,536		

The calculated temperature values at the nodes are presented in table 1. These data reflect the discrete temperature distribution along the length of the rod and enable a detailed analysis of the thermal state of the structure, taking into account the specified boundary conditions, including heat fluxes and convective heat transfer.

 ISSN 2723-6471

Analysis of the results shows that the temperature field is significantly non-uniform. In the initial section of the rod (nodes 1–3), a gradual decrease in temperature is observed from 134.787°C to 101.821°C. This behavior is due to the negative heat flux at the left end, which leads to heat removal from the system.
In the middle section of the rod (nodes 4–8), a significant increase in temperature is recorded, reaching a maximum of 305.514°C at node 8. This sharp increase is due to the combined effect of the material's thermal conductivity and the boundary conditions, including localized thermal effects and partial thermal insulation. The presence of a pronounced temperature peak indicates the formation of a heat concentration zone.
At the right end of the rod (nodes 8–11), the temperature decreases again, reaching 208.101°C at node 11. This is explained by the effect of convective heat exchange with the environment, determined by the heat transfer coefficient and the ambient temperature. This mechanism leads to cooling of the rod and a smoothing of the temperature profile.
Particular attention should be paid to the presence of significant temperature gradients, primarily in the middle section of the rod (nodes 5–8). These gradients are of fundamental importance, as they determine the level of thermal stress that occurs. Areas with the greatest temperature differences are potentially the most dangerous in terms of the strength and durability of the structure under thermomechanical loading
Table 1provides a more detailed view of the nodal temperature values obtained by numerically solving the system of equations for a rod divided into five finite elements. It is evident that the temperature changes unevenly along the rod's length, due to the specified boundary conditions and thermal effects, with the greatest changes observed near the areas of heat flux application or heat exchange. The obtained results are consistent with the temperature distribution law shown in figure 2 and clearly confirm the nature of the temperature field changes along the rod.

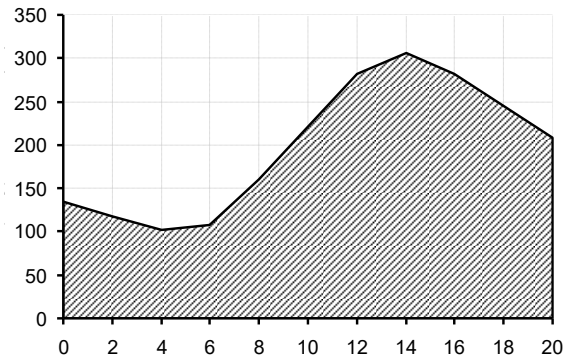

Figure 2. Temperature distribution law for n=5 KE

In this case, the area of the bounded curve is $T = T(x)$ and the coordinate axes OT and Ox will be $S_{T1} = 3989{,}96(\,^{\circ}C \times см)$. Then the magnitude of the elongation of the rod under consideration due to thermal expansion will be $\Delta\ell_{T1} = 0{,}04987(см)$.

Table 2 contains the nodal temperature values obtained by numerically solving the variational problem (12) using the finite element method, partitioning the rod into twenty quadratic elements (NQE = 20). In this case, the computational model includes 41 nodes, providing a significantly higher degree of spatial resolution of the temperature field compared to previous discretization options. Increasing the number of finite elements leads to a more precise temperature distribution and allows for a more detailed reflection of local features of thermal processes, including zones of intense heat transfer and regions with maximum temperature gradients.

Table 2. Temperature value (number of quadratic elements in the rod NQE =20)

Node. Dots	Temp. in knots. Dots $T(\,^{\circ}C)$	Node. Dots	Temp. in knots. Dots $T(\,^{\circ}C)$	Node. Dots	Temp. in knots. Dots $T(\,^{\circ}C)$	Node. Dots	Temp. in knots. Dots $T(\,^{\circ}C)$
1	135,615	11	100,614	21	220,100	31	299,071
2	130,857	12	103,309	22	234,851	32	292,603
3	126,099	13	108,495	23	249,601	33	283,318
4	121,773	14	115,838	24	263,430	34	273,203

 ISSN 2723-6471

5	117,447	15	126,054	25	277,259	35	263,088
6	113,497	16	138,617	26	288,712	36	253,504
7	109,547	17	154,779	27	297,088	37	243,921
8	105,926	18	171,672	28	302,031	38	234,829
9	102,305	19	188,565	29	303,989	39	225,738
10	100,226	20	204,333	30	302,979	40	217,100
						41	208,463

In table 2, we see that the initial section of the rod (nodes 1-10) shows a steady and almost monotonous decrease in temperature from 135.615 °C to 100.226°C. This region is characterized by a smooth temperature profile without sharp jumps, indicating the dominant influence of the specified negative heat flux at the left end. The minimum temperature is reached at node 10, corresponding to the region of greatest cooling.

A zone of intense temperature increase forms in the range of nodes 10–30. After reaching the minimum, a gradual and then accelerated increase in temperature begins, associated with thermal conductivity processes and the redistribution of thermal energy within the rod. A particularly pronounced temperature increase is observed in the region of nodes 15–25, reflecting the presence of significant temperature gradients. The maximum temperature is recorded at node 29 and is 303.989°C. However, unlike the more coarse model (NQE = 5), the maximum distribution becomes smoother, indicating increased accuracy of the numerical solution.

At the end of the rod (nodes 30–41), a gradual decrease in temperature is observed from 302.979°C to 208.463°C. This decrease is due to the influence of convective heat exchange with the environment, determined by third-order boundary conditions. The temperature field in this zone has a smooth downward slope, indicating stabilization of the thermal regime and the absence of localized overheating.

The corresponding temperature distribution field along the rod is illustrated in figure 3, reflecting a highly refined and smooth temperature profile obtained with the increased number of elements. The integral characteristics in this case are $S_{T3} = 3969{,}239(\ ^{\circ}C \times cm)$, representing the cumulative thermal effect, and $\Delta\ell_{T3} = 0{,}0496cm,$ which characterizes the thermal elongation of the rod. These values indicate further convergence of the solution and confirm that increasing the number of elements leads to more precise and stable results.

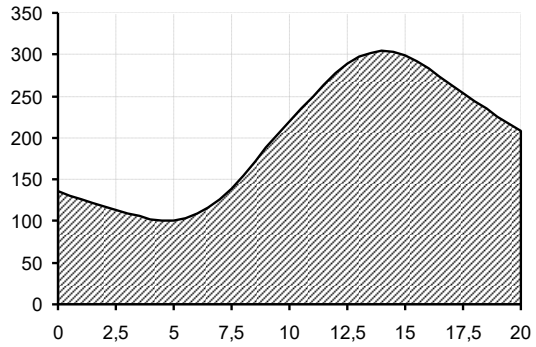

Figure 3. Temperature distribution law for n=20 KE

Compared to (S_{T1},$\Delta\ell_{T1}$) these values are 0.519% less. As you can see, this difference is not big.

Table 3 presents the nodal temperature values obtained after discretizing the rod into 100 quadratic elements, resulting in a total of 201 nodes. This discretization allows for a highly accurate representation of the temperature distribution, minimizing numerical errors and ensuring solution convergence. The obtained values can be considered as reference values for analyzing the effect of the degree of discretization on the result.

Table 3. Temperature value (number of quadratic elements in the rod NQE =100)

Node. dots	**Temp. in knots points**	**Node. dots**	**Temp. in knots points**	**Node. dots**	**Temp. in knots points**	**Node. dots**	**Temp. in knots points**

 ISSN 2723-6471

	$T(^{\circ}C)$		$T(^{\circ}C)$		$T(^{\circ}C)$		$T(^{\circ}C)$
1	135,705	51	100,586	101	219,795	151	299,038
2	134,715	52	100,942	102	222,824	152	297,946
3	133,725	53	101,396	103	225,853	153	296,739
4	132,755	54	101,940	104	228,842	154	295,434
5	131,784	55	102,581	105	231,831	155	294,014
6	130,832	56	103,310	106	234,781	156	292,499
7	129,880	57	104,138	107	237,731	157	290,871
8	128,947	58	105,054	108	240,643	158	289,149
9	128,013	59	106,070	109	243,555	159	287,316
10	127,098	60	107,172	110	246,429	160	285,391
20	118,358	70	123,621	120	274,271	170	265,098
30	110,382	80	151,009	130	295,496	180	245,822
40	103,073	90	184,965	140	303,729	190	227,538
50	100,321	100	216,725	150	300,028	200	210,170
						201	208,477

In table 3, we see that in the initial part of the rod (nodes 1-50), there is a smooth and almost linear decrease in temperature from 135.705°C to 100.321°C. Unlike more coarse grids, the temperature field here changes without jumps, demonstrating physically correct behavior. This is due to the negative heat flux at the left end, which causes stable heat dissipation.

The minimum temperature value is recorded near nodes 50–51 (≈100.3–100.6°C), which corresponds to the transition zone between the cooled region and the subsequent heating zone. Due to the high mesh density, this region is determined with high accuracy, without artificial bias.

A zone of intense temperature increase forms in the central part of the rod (nodes 50–150). Starting from the minimum value, the temperature initially increases gradually, then the increase becomes more pronounced. A particularly noticeable increase is observed in the range of nodes 80–130, where the temperature rises from ~151°C to ~295°C. This indicates the presence of significant temperature gradients associated with the redistribution of thermal energy within the rod.

The maximum temperature is reached in the region of nodes 140–150 and is approximately 303.7°C (node 140). It is important to note that the maximum is smoothed: the temperature at adjacent nodes changes only slightly, indicating the absence of numerical artifacts and confirming the stability of the solution.

In the terminal part of the rod (nodes 150–201), a gradual decrease in temperature is observed from ~300°C to 208.477°C. This region reflects the influence of convective heat exchange with the environment. The temperature field decreases smoothly, without sharp changes, indicating correct modeling of third-order boundary conditions.

The analysis of temperature gradients is particularly important. At NQE = 100, the gradient distribution becomes maximally smooth and physically realistic. The largest gradients are observed in the central zone (approximately nodes 90–130), which corresponds to the region of potential maximum thermal stress.

The corresponding temperature distribution along the length of the rod is shown in figure 4, illustrating an almost fully converged and smooth temperature profile. The obtained integral values are $S_{T4} = 3967{,}919(\ ^{\circ}C \times cm)$ and $\Delta\ell_{T4} = 0{,}049599(cm)$, which characterize the overall thermal effect and the resulting thermal elongation, respectively. In comparison with $(S_{T1}, \Delta\ell_{T1})$, the difference is only about 0.5525%, indicating that further mesh refinement leads to negligible changes and confirming the high accuracy and stability of the numerical solution.

 ISSN 2723-6471

Figure 4. Temperature distribution law for n=100 KE

This level of discretization ensures a sufficiently accurate approximation of the temperature field along the rod while maintaining computational efficiency. The obtained nodal temperatures in table 4 provide the basis for reconstructing the continuous temperature distribution. Furthermore, the results can be used for subsequent thermal stress analysis and validation of the numerical model.

Table 4. Temperature value (number of quadratic elements in the rod NQE =200)

Node. dots	Temp. in knots points $T(^{\circ}C)$	Node. dots	Temp. in knots points $T(^{\circ}C)$	Node. dots	Temp. in knots points $T(^{\circ}C)$	Node. dots	Temp. in knots points $T(^{\circ}C)$
1	135,708	101	100,585	201	219,785	301	299,037
2	135,211	102	100,752	202	221,305	302	298,503
3	134,713	103	100,943	203	222,824	303	297,941
4	134,221	104	101,157	204	224,334	304	297,354
5	133,728	105	101,395	205	225,843	305	296,739
10	131,309	110	102,933	210	233,301	310	293,269
20	126,640	120	107,761	220	247,862	320	284,385
30	122,190	130	114,976	230	261,959	330	274,113
40	117,942	140	124,713	240	275,615	340	264,106
50	113,883	150	137,190	250	287,602	350	254,366
60	110,001	160	152,707	260	296,205	360	244,882
70	106,285	170	169,943	270	301,562	370	235,645
80	102,724	180	186,604	280	303,815	380	226,646
90	100,327	190	202,698	290	303,100	390	217,874
100	100,441	200	218,255	300	299,545	400	209,322
						401	208,477

The table 4 shows an increase in the density of the finite element grid compared to the previous sampling options (NQE = 5, 20, 100) leads to a further refinement of the temperature profile and actually allows us to consider the resulting solution as limiting (convergent).

In the initial region of the rod (nodes 1–100), a smooth and strictly monotonic temperature decrease from 135.708°C to 100.441°C is observed. The temperature field in this zone is characterized by high smoothness and the absence of any numerical fluctuations. This behavior is due to the negative heat flux at the left end, which ensures stable heat dissipation. The minimum temperature value is recorded near nodes 90–110 (≈100.3–100.6°C), which determines the location of the transition zone with high accuracy.

In the central part of the rod (nodes 100–300), a region of intense temperature increase forms. After reaching the minimum, the temperature begins to increase, initially smoothly, then with increasing velocity. A particularly pronounced increase is observed in the range of nodes 140–260, where the temperature varies from ~125°C to ~296°C. The maximum temperature is reached in the range of nodes 270–280 and is approximately 303.8°C (node 280). The maximum is smooth: adjacent temperature values differ only slightly, indicating the high accuracy of the numerical solution and the absence of discretization artifacts.

At the end of the rod (nodes 300–401), a gradual decrease in temperature is observed from ~299.5°C to 208.477°C. This region reflects the influence of convective heat exchange with the environment. The temperature field decreases uniformly, without sharp gradients, confirming the correctness of the third-kind boundary conditions and their numerical implementation.

An analysis of temperature gradients shows that the most significant temperature changes are concentrated in the central zone (approximately nodes 150–250). It is in this region that the maximum temperature gradients form, identifying the most potentially hazardous zones in terms of thermal stress. Unlike coarser meshes, with NQE = 200, the gradient distribution is completely smoothed and physically justified.

In this case, the temperature distribution field is shown in figure 5. Also, the values (S_{T5},$\Delta\ell_{T5}$) are given as $S_{T5} = 3967{,}878(\ ^{\circ}\mathrm{C} \times cm)$ and $\Delta\ell_{T5} = 0{,}0495984748(cm)$. These results indicate a slightly more refined solution compared to the previous approximation. When compared with (S_{T1},$\Delta\ell_{T1}$), the obtained values are lower by 0.5535%, which demonstrates the convergence of the numerical solution with mesh refinement.

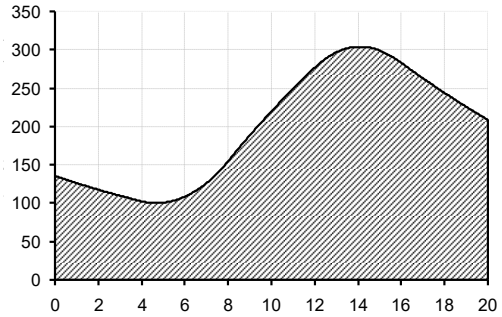

Figure 5. Temperature distribution law for n=200 KE

Thus, from the numerical experiments conducted, it is clear that in engineering calculations it is possible to limit oneself to a minimum number of discrete quadratic elements. The calculation results show that the general nature of the temperature distribution is preserved for all discretization options. The temperature field is distinctly nonlinear and includes three characteristic zones: an initial decrease in temperature, a subsequent rapid increase with the formation of a maximum, and a further decrease near the right end. This behavior is determined by the combined effects of the specified heat fluxes, heat exchange with the environment, and the thermal conductivity of the material. Thus, the study demonstrates that the choice of discretization has a significant impact on the accuracy of numerical simulations with a small number of elements; however, once a certain level of detail is reached, the solution stabilizes. The obtained results confirm the effectiveness of using quadratic finite elements for modeling thermal conductivity in beam systems and provide a reliable basis for subsequent analysis of the thermal stress state of the structure.

5. Discussion

The results obtained demonstrate that the proposed numerical approach provides a stable and convergent solution for thermomechanical analysis of a rod with a variable cross-section under difficult thermal boundary conditions. In particular, the discretization of the rod into 200 quadratic finite elements allowed us to obtain a system of 401 equations that allows us to accurately determine the temperature values at the nodes and the corresponding temperature distribution along the rod. The smoothed profile of the temperature field (Fig. 1). 6) confirms that the use of higher-order approximating functions ensures continuity and improves the quality of the solution compared to lower-order methods.

A key indicator of the reliability of the numerical model is the convergence of integral characteristics such as S_T and thermal elongation $\Delta\ell_T$. The obtained values $S_{T5} = 3967{,}878(\ ^{\circ}\mathrm{C} \times cm)$ and $\Delta\ell_{T5} = 0{,}0495984748(cm)$ differ from the reference solution by only 0.5535%, which indicates good agreement and numerical stability. This small

deviation suggests that further mesh refinement would lead to diminishing improvements, confirming the efficiency of the chosen discretization level.

The results also reveal pronounced variable geometry and mixed thermal boundary conditions for temperature. Unlike simplified models with contoured cross-sections, this formulation exhibits localized temperature gradients caused by partial thermal insulation and non-uniform heat flows. These effects are critical for practical applications, as if improperly accounted for, they can lead to structural stresses and reliable failure. Compared to existing studies, which primarily use uniform and simplified boundary conditions, the proposed approach provides a more realistic representation of service conditions. The integration of convective heat transfer, internal heat transfer, and geometric variability within a single computational framework expands the predictive capabilities of the models.

However, some limitations should be noted. The current model is based on one-dimensional collisions and does not explicitly consider multidimensional effects or material nonlinearities arising from those included in the formulation. Future research could focus on expanding the range of fully compatible 3D problems, including material properties, temperature determination, and model validation against experimental data. Overall, the presented results confirm the effectiveness of the developed method and its potential applicability to the engineering design and analysis of thermally loaded beam structures.

6. Conclusion

This method studied the transient thermomechanical behavior of a finite-length rod with variable cross-section under complex thermal conditions, including partial thermal insulation, local heat flow, and heat exchange with the environment. A mathematical model based on the energy conservation principle was developed to determine the temperature, thermal expansion, axial rotation, and the normal (deflected) state of the rod.

The results demonstrate that nonuniform boundary conditions and geometric variability affect the temperature field and, consequently, the distribution of thermal and mechanical stresses. It is shown that accurately determining the temperature profile is crucial for measuring the thermomechanical state of structural elements and ensuring the reliability of engineering systems operating under high-temperature conditions.

A computational algorithm and software package were developed for analyzing the rod by breaking it down into finite elements and systematically monitoring heat transfer conditions, startup defects, and internal heat sources. The approach enables flexible modeling of various thermal landscapes, including mixed boundary conditions and spatially variable material properties.

The results confirm that the proposed method provides a consistent and effective way to predict temperature fields and boundaries using thermomechanical methods. It also addresses design, safety, and the exclusion of structural elements in energy and other temperature-sensitive applications. Furthermore, the developed framework can be extended to more complex systems and serve as a foundation for future research in the field of advanced thermomechanical analysis.

7. Declarations

7.1. Author Contributions

Conceptualization: Z.A. and S.A.; Methodology: S.A.; Software: Z.A.; Validation: Z.T. and E.N.; Formal Analysis: Z.A. and S.A.; Investigation: Z.T.; Resources: S.A.; Data Curation: S.A.; Writing Original Draft Preparation: Z.T., and E.N.; Writing Review and Editing: S.A. and E.N.; Visualization: Z.A.; All authors have read and agreed to the published version of the manuscript.

7.2. Data Availability Statement

The data presented in this study are available on request from the corresponding author.

7.3. Funding

The authors received no financial support for the research, authorship, and/or publication of this article.

7.4. Institutional Review Board Statement

Not applicable.

7.5. Informed Consent Statement

Not applicable.

7.6. Declaration of Competing Interest

The authors declare that they have no known competing financial interests or personal relationships that could have appeared to influence the work reported in this paper.

References

[1] S. P. Timoshenko and J. N. Goodier, Theory of Elasticity, 3rd ed. New York, NY, USA: McGraw-Hill, 1970. doi:10.1002/zamm.19720520317.

[2] B. F. Shorr, "Thermoelasticity," in Thermal Integrity in *Mechanics and Engineering, Berlin, Germany: Springer*, 2015, pp. 33–56. doi:10.1007/978-3-662-46968-2_2.

[3] A. C. Eringen, Mechanics of Continua. New York, NY, USA: Wiley, 1967. doi:10.1002/zamm.19680480529.

[4] H. M. Ma and J. Wang, "Nonlinear thermoelastic analysis of superconductors," *Applied Mathematics and Mechanics*, vol. 30, no. 3, pp. 321–330, 2009. doi: 10.1007/s10483-009-0305-6.

[5] G. Griffith, S. Tucker, J. Milsom, and G. Stone, "Problems with modern air-cooled generator stator winding insulation," *IEEE Electrical Insulation Magazine*, vol. 16, no. 6, pp. 6–10, 2000. doi:10.1109/57.887599.

[6] Y. Li, "Investigation of heat transfer characteristics on rod fastening rotor," *IOP Conference Series: Materials Science and Engineering*, vol. 677, no. 3, Art. no. 032032, pp.1-12, 2019. doi:10.1088/1757-899X/677/3/032032.

[7] K. Shibib, M. Minshid, and N. Alattar, "Thermal and stress analysis in Nd:YAG laser rod with different double end pumping methods," *Thermal Science*, vol. 15, no. 2, pp. 399–407, 2011. doi:10.2298/TSCI101201004S.

[8] V. Andreev and R. Turusov, "Nonlinear modeling of the kinetics of thermal stresses in polymer rods," *in Advanced Materials and Structural Engineering, Boca Raton, FL, USA: CRC Press*, vol. 2016, no. Jan., pp. 719–722, Jan. 2016. doi:10.1201/b20958-150.

[9] T. Belytschko, W. K. Liu, and B. Moran, Nonlinear Finite Elements for Continua and Structures. Chichester, U.K.: Wiley, 2000. doi:10.1002/9780470316511.

[10] T. W. Wright, The Physics and Mathematics of Adiabatic Shear Bands. Cambridge, U.K.: Cambridge University Press, 2002. doi:10.1017/CBO9780511535086.

[11] R. C. Batra, Elements of Continuum Mechanics. Reston, VA, USA: AIAA, 2006. doi:10.2514/4.861765.

[12] D. H. Sukarno, "Analysis of nuclear fuel rod temperature distribution using CFD calculation and analytical solution," *AIP Conference Proceedings,* vol. 2331, no. 1, pp. 1–10, 2021. doi:10.1063/5.0058888.

[13] J. M. El-Azab, H. M. Kandel, M. A. Khedr, and H. M. El-Ghandoor, "Numerical study of transient temperature distribution in passively Q-switched Yb:YAG solid-state laser," *Optics and Photonics Journal*, vol. 4, no. 3, pp. 46–53, 2014. doi:10.4236/opj.2014.43007.

[14] S. Kou, Welding Metallurgy, 2nd ed. Hoboken, NJ, USA: Wiley, 2003. doi:10.1002/0471434027.

[15] A. Mishchenko, "Spatial problem of the stressed-deformed state of a structurally inhomogeneous rod," *IOP Conference Series: Materials Science and Engineering*, vol. 953, no. 1, pp. 1–10, 2020. doi:10.1088/1757-899X/953/1/012004.

[16] J.-K. Hwang, "Thermal behavior of a rod during hot shape rolling and its comparison with a plate during flat rolling," *Processes*, vvol. 8, no. 3, pp. 1–17, 2020. doi:10.3390/pr8030327.

[17] D. L. Logan, A First Course in the Finite Element Method, 5th ed. Boston, MA, USA: Cengage Learning, 2012. doi:10.1007/978-1-4899-7550-8.

[18] Q. Liu and X. He, "Thermal analysis of Terfenol-D rods with different structures," *Micromachines*, vol. 14, no. 1, pp. 1–14, 2023. doi:10.3390/mi14010216.

[19] J. C. A. Gaspar Jr., M. L. Moreira, and P. A. B. Desampaio, "Temperature distribution on fuel rods: Effect of eccentricity in UO_2 pellets," *Annals of Nuclear Energy*, vol. 38, no. 12, pp. 2730–2736, 2011. doi:10.1016/j.anucene.2011.07.016.

[20] Z. Tashenova, E. Nurlybaeva, and A. Kudaykulov, "Method preparation and solution algorithm for resolving stationary problem of a rod under thermo-stressed condition," *Advanced Materials Research*, vols. 875–877, no.1, pp. 858–862, 2014. doi:10.4028/www.scientific.net/AMR.875-877.858.

[21] Z. H. M. Tashenova, E. N. Nurlybaeva, and A. K. Kudaikulov, "Method of solution and computational algorithm for mixed thermo-mechanics problem," *World Applied Sciences Journal,* vol. 28, no. 12, pp. 2113–2119, 2013. doi:10.5829/idosi.wasj.2013.28.12.422.

[22] Z. M. Tashenova, E. N. Nurlybaeva, and A. K. Kudaiykulov, "Method of solution and computational algorithm for mixed thermo-mechanics problem," *World Applied Sciences Journal*, vol. 22, Special Issue 2, no.1, pp. 49–57, 2013. doi:10.5829/idosi.wasj.2013.22.tt.22139.

[23] Z. H. M. Tashenova, A. K. Zhumadillaeva, E. N. Nurlybaeva, and A. K. Kudaykulov, "Numerical study of established thermo-mechanical state of rods," *Advanced Science Letters*, vol. 19, no. 8, pp. 2395–2397, 2013. doi:10.1166/asl.2013.4926.

[24] K. K. Gornostaev, A. V. Kovalev, and Y. V. Malygina, "Stress–strain state in an elastoplastic pipe considering temperature and compressibility," *Journal of Physics: Conference Series*, vol. 973, Art. no. 012032, no. 1, pp.1-12, 2018. doi:10.1088/1742-6596/973/1/012032.

[25] B. F. Shorr, "Foundations of thermoelasticity," in Thermal Integrity in Mechanics and Engineering, Berlin, Germany: *Springer*, 2015, pp. 33–55. doi:10.1007/978-3-662-46968-2_2.

[26] O. C. Zienkiewicz and R. L. Taylor, The Finite Element Method, 5th ed. Oxford, U.K.: Butterworth-Heinemann, 2000. doi:10.1016/B978-075066320-0/50001-5.